www.czasopisma.pan.pl PAN POLSKA AKADEMIA NAUK www.journals.pan.pl

PAN POLSKA AKADEMIA NAUK

JOURNAL OF WATER AND LAND DEVELOPMENT

e-ISSN 2083-4535

ITP-PIB

Polish Academy of Sciences (PAN) Institute of Technology and Life Sciences – National Research Institute (ITP – PIB)

JOURNAL OF WATER AND LAND DEVELOPMENT
DOI: 10.24425/jwld.2021.139940
2022, No. 52 (I–III): 27–33

Spatiotemporal mapping of inundation area at Lake Limboto in Gorontalo, Indonesia, using cloud computing technology

Rakhmat Jaya Lahay ✉, Syahrizal Koem

Universitas Negeri Gorontalo, Department of Earth Science and Technology, B.J Habibie Street, Bone Bolango, 96183, Gorontalo, Indonesia

RECEIVED 22.10.2020 REVIEWED 10.12.2020 ACCEPTED 26.04.2021

Abstract: Monitoring activities on the dynamics of water shrinkage at Lake Limboto are essential to the lake's ecosystem's recovery. A remote sensing technology functions to monitor the dynamics of lake inundation area; this allows one to produce a comprehensive set of spatial and temporal data. Such complex satellite dataset demands extra time, greater storage resources, and greater computing capacity. The Google Earth Engine platform emerges as the alternative to tackle such problems. The present study aims to explore the capability of Google Earth Engine in formulating spatial and temporal maps of the inundation area at Lake Limboto. A total of 345 scenes of Landsat image on the study area (available during the period of 1989–2019) were involved in generating a quick inundation area map of the lake. The whole processes (pre-processing, processing, analysing, and evaluating) were automatized by using the Google Earth Engine interface. The evaluation of mapping result accuracy indicated that the average score of F1-score and Intersection over Union (IoU) was at 0.88 and 0.91, respectively. Moreover, the mapping results of the lake's inundation area from 1989 to 2019 showed that the inundation area tended to decrease significantly in size over time. During the period, the lake's area also shrank from 3023.8 ha in 1989 to 1275.0 ha in 2019. All in all, the spatiotemporal information about the changes in lake area may be treated as a reference for decision-making processes of lake management in the future.

Keywords: Google Earth Engine, Lake Limboto, lake shrinkage, Landsat, remote sensing, water index

INTRODUCTION

The problem of surface area shrinkage at Lake Limboto, as reported by Subehi *et al.* [2016], has developed into an alarming state. The shrinkage is mainly caused by sedimentation that enters the lake at a massive rate [JICA 2002]. The alarming negative impacts of the shrinkage have raised serious concerns about the urgency to monitor the dynamics of the lake's environment [Putra *et al.* 2013]. A remote sensing technology is applicable in monitoring the dynamics of lake surface water to yield variability of spatial and temporal information in continuous manner [Huang *et al.* 2018]. The spatiotemporal information functions as the supporting data in formulating lake management decisions. That being mentioned, activities of lake monitoring have been incorporated into the priority list of the Lake Limboto ecosystem recovery program carried out by the national and regional governments [KLHK 2015].

Previous studies have discussed the utilisation of remote sensing satellite data in mapping out the dynamics of land and water resources [Acharya *et al.* 2018; Bolanos *et al.* 2016; Dinka, Chaka 2019; Eraku *et al.* 2019; Hardy *et al.* 2019; Rezzag Bara *et al.* 2019]. The aforementioned studies, however, only addressed the implementation of satellite images in a short period or with limited numbers of images (i.e., one scene) [Nguyen *et al.* 2019]. On top of that, despite involving computer software, the existing literature still uses a conventional method of image processing. The limitations found in previous studies have been addressed by more recent studies that incorporated cloud computing technology [Wang *et al.* 2020].

The present work lays its basis on the notion that remote sensing satellite technology has been implemented to produce the satellite image data of Lake Limboto from 1989 to 2019. The recording process has yielded numbers of satellite images available for data processing. Such large-sized images, if down-

loaded and processed manually, will require longer time to execute. Therefore, a platform that features the optimal capability of storing and computing such datasets is highly substantial to automatize the image downloading and processing activity. One of the geospatial platforms that are capable of accommodating such needs is Google Earth Engine or GEE [Gorelick *et al.* 2017]. As a cloud-based platform, GEE features a high computing performance to process and analyse large-sized geospatial data [Kumar, Mutanga 2018]. The platform is also supported by a web interface environment that enables the users to access wide ranges of remote sensing image data stored within existing public catalogs without having to download them [Gorelick *et al.* 2017]. It is worth noting, however, that the implementation of such a technology in monitoring activities of the dynamics of land and water resources is still limited and thus becomes an open field for exploration [Tamiminia *et al.* 2020].

The present work aims to explore the GEE platform's performance in mapping out the spatiotemporal variabilities of Lake Limboto inundation from 1989 to 2019. Regarding that, the study relies on the GEE to access the Landsat images, conduct image processing procedures, and evaluate the mapping results. Within this study, all available Landsat images within the period of 1989–2019 in the GEE catalog are involved in extracting the Limboto Lake inundation area by applying the water index algorithm. On top of that, the preprocessing, processing, and analysis procedures are automatized by using the GEE interface. The mapping results are then juxtaposed with the data produced by Global Surface Water within the period of 1994–2019 available in the GEE catalog.

MATERIALS AND METHODS

STUDY AREA

The research study area encompassed Lake Limboto and its surroundings (Fig. 1), located in Gorontalo province, on the north side of Sulawesi Island. The overall area size is 910.04 km^2 in size [Putra *et al.* 2013]. The lake holds water from 23 rivers located on the south, west, and north side of the lake. The lake's inundation area is formed by five mainstem rivers, viz., Rintenga, Alopohu, Marisa, Meluopo, and Biyonga. The lake's runoff flows to the Gorontalo bay through Tapodu River, located at the southeast end of the lake [JICA 2002; Yunginger *et al.* 2018].

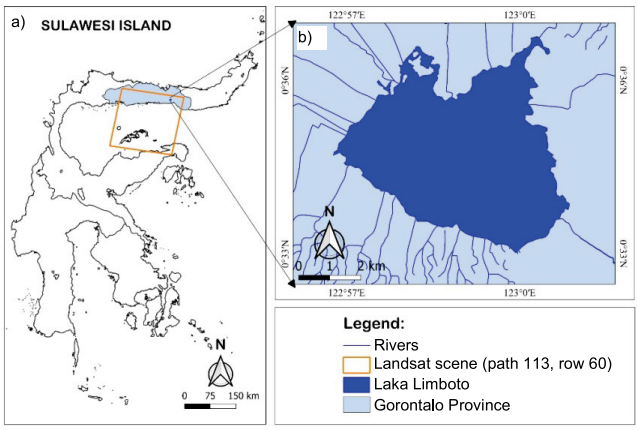

Fig. 1. Study area: a) Sulawesi Island, b) Lake Limboto; source: own elaboration

GEOSPATIAL DATASET

The study employed datasets from Landsat imagery and data produced by Global Surface Water. Both datasets are accessible in the GEE's images collection public catalog [Gorelick *et al.* 2017]. From the Landsat image collections, the study involved TM, ETM+, and OLI Top-of-Atmosphere (ToA) reflectance (path 113 and row 60) from 1 January 1989 to 31 December 2019 (Tab. 1). The Landsat optical images were applied because the data are available for free with 30 m spatial resolution and 16-days temporal resolution. In addition to that, the Landsat satellite images were commonly applied in monitoring the dynamics of surface water for a long duration, as conducted by Huang *et al.* [2018], Wang *et al.* [2018] and Wang *et al.* [2019]. Along with the Landsat imagery dataset, the study also involved datasets from Global Surface Water by the European Commission's Joint Research Centre (JRC), i.e., JRC Yearly Water Classification History (currently available in v1.2) [Pekel *et al.* 2016]. The dataset from Global Surface Water was used to evaluate the lake inundation map yielded by the GEE platform.

Table 1. Image collections used in this study

Dataset	Time (DD.MM. YYYY)	Image count	Application
Landsat 4 TM images	10.04.1989–10.01.1991	3	inundated area mapping
Landsat 5 TM images	26.05.1991–21.07.2000	39	
Landsat 7 ETM+ images	02.12.1999–30.03.2014	143	
Landsat 8 OLI images	20.04.2013–30.09.2020	160	
JRC Yearly Water Classification History (v1.2) images	1991–2019	–	result evaluation

Source: own elaboration.

DATA PRE-PROCESSING

GEE is a cloud-based computing application that provides facilities for scientific research and access to many remote sensing datasets [Tamiminia *et al.* 2020]. This platform can be accessed via a web browser connected to the internet. This application has an interface in the form of a code editor that allows users to develop the algorithms of remote sensing dataset processing [Amani *et al.* 2020]. Therefore, all image processing steps in this study were written in the JavaScript programming language through the code editor panel in GEE.

The pre-processing was conducted in the following steps: firstly, the authors accessed the Landsat images in the GEE's catalog, filtered the image based on path and row, and determined the study area coverage. A total of 345 scenes of Landsat images from different sensors (TM, ETM+, and OLI) were accessed through the GEE's catalog. These images were available as image collections and had the same spatial resolution of 30 m × 30 m. From 2013 through 2019, as the Landsat 8 OLI began to operate, the images produced were relatively high in number. It is worth

noting that the image data in 1992–1993 were not available in the GEE catalog.

Following the above step was the application of a cloud-masking function by appointing a cloud score to every pixel in the image. This function is available in GEE to mask pixels in each image that has a cloud score value greater than a threshold. In this study, the threshold was set at 20. The threshold value was determined based on subjective interpretation [Okoro *et al.* 2016]. The final stage in the preprocessing was the calculation of Normalized Difference Water Index (*NDWI*) [McFeeters 1996] and Normalized Difference Vegetation Index (*NDVI*) [Rouse *et al.* 1973] using the formula in Table 2. The *NDWI* and *NDVI* have been used in previous studies to detect water features and vegetation using satellite data [Wang *et al.* 2018]. The misclassification of mixed objects (vegetation-water) by *NDWI* could be minimised by using *NDVI* [Wang *et al.* 2019]. This water index calculation was applied to each image.

Table 2. The formula of water indices used for water feature extraction

Index	Formula	Reference
NDWI	*NDWI* = (green – NIR) / (green + NIR)	McFeeters [1996]
NDVI	*NDVI* = (NIR – red) / (NIR + red)	Rouse *et al.* [1973]

Explanations: *NDWI* = Normalized Difference Water Index, *NDVI* = Normalized Difference Vegetation Index, NIR = near-infrared.
Source: own elaboration.

Based on the *NDWI* and *NDVI* formula in Table 2, the near-infrared (NIR) referred to the near-infrared band score, while the green referred to the green band score, and red referred to the red band score in the Landsat images. The water feature in the *NDWI* score will yield a positive score [McFeeters 1996], while that in *NDVI* will yield a negative score [Rouse *et al.* 1973]. The final outputs of the stage were *NDWI* and *NDVI* image collection.

INUNDATED AREA MAPPING

The *NDWI* and *NDVI* image collection retrieved from the previous stage comprised series of observations. One year of the set would consist of several images. Thus, one would require to compose the images resulted within a year into a single image that represents the particular year. The process was conducted by applying the join and quality mosaic methods available in the GEE platform. The methods were chosen because the images were collected at different times, so this affected the pixel value of an object [Google Earth Engine 2020]. The quality mosaic method composited images based on the maximum *NDVI* and *NDWI* values so that a cloud-free image was obtained [Stuhler *et al.* 2016]. A composite image for each period was generated from this process.

The composed image was then used to extract the inundation area by classifying the image pixels into two classes, i.e., water and non-water area. The classification needs a threshold value, by which this study applied the Otsu method [Otsu 1979]. In previous studies, the threshold value for *NDVI* and *NDWI* was zero [McFeeters 1996; Rouse *et al.* 1973]. In that regards, adjustment of the threshold value based on the pixel image value can improve classification accuracy [Buma *et al.* 2018].

The Otsu method works with the assumption that the image contains two classes in which the pixel histogram has a bimodal distribution. The threshold value is obtained by finding a single value that separates the two classes based on the largest variance between classes [Du *et al.* 2016]. In this study, the calculation of the threshold value was generated dynamically and automatically through the GEE's interface by adapting the JavaScript code written by Clinton [2017]. These calculations were applied to *NDVI* and *NDWI* images, respectively. Based on this threshold value, an extraction process was carried out to separate water and non-water. The criteria "*NDWI* > threshold and *NDVI* < threshold" were used to classify objects as water or non-water. Pixels that match the criteria were classified as water. The output of this process was maps of inundation areas from 1989 to 2019 and annual inundation area values. Further, the authors applied a long-term trend test by employing a Mann–Kendall test [Kendall 1975; Mann 1945] to identify the presence of a monotonic trend (increasing or decreasing). Sen's method was also applied to calculate the true slope of the trend [Sen 1968]. These two tests were done by using Excel software.

ACCURACY ASSESSMENT

An accuracy assessment to evaluate the mapping results of the inundation area was conducted by applying the confusion matrix approach. The confusion matrix provides information of comparison between the prediction result and reference image [Buma *et al.* 2018; Maxwell, Warner 2020]. As for the reference image, the authors involved JRC Yearly Water Classification History images available in the GEE catalog. The "Permanent Water" attribute class at the JRC data was selected to be compared with the "Water" class at the mapping results. Since the 1989–1993 JRC data was unavailable, the comparison was only performed for the mapping results in the period of 1994–2019. The comparison results in the form of a confusion matrix were then applied as a reference to calculate the performance criteria. Since only two classes were involved (water and non-water), the calculated performance criteria only consisted of Producer's Accuracy (PA), User's Accuracy (UA), F1-score, and Intersection over Union (IoU) [Maxwell, Warner 2020; Wang *et al.* 2020]. The accuracy assessment results (consisting of four performance criteria) were made for each annual image based on the classification results in the period of 1994–2019.

RESULTS

PERFORMANCE EVALUATION RESULTS

Table 3 displays the results of performance evaluation, consisting of Producer's Accuracy (PA), User's Accuracy (UA), F1-score, and Intersection over Union (IoU). The evaluation was conducted for 26 images as the extraction result of the Lake Limboto inundation area from 1994 to 2019. As shown in Table 3, in F1-score criteria, 22 of 26 images arrived at 0.80–0.97 range, while the rest four images were at 0.64–0.79 range. Meanwhile, in IoU criteria, 25 images arrived at 0.80–0.98 range. The results of the performance evaluation show that the results of inundated area extraction are consistent with the reference map.

Table 3. Results of performance evaluation for each image based on the classification results from 1994 to 2019

Year	Evaluation acc. to			
	PA	UA	F1-score	IoU
1994	0.97	0.95	0.96	0.97
1995	0.98	0.89	0.93	0.94
1996	0.94	0.87	0.91	0.92
1997	0.96	0.88	0.92	0.94
1998	0.97	0.96	0.96	0.97
1999	0.98	0.87	0.92	0.93
2000	0.96	0.83	0.89	0.89
2001	0.99	0.80	0.89	0.87
2002	0.98	0.94	0.96	0.96
2003	0.99	0.96	0.97	0.98
2004	0.96	0.92	0.94	0.95
2005	0.97	0.93	0.95	0.96
2006	0.90	0.89	0.90	0.91
2007	0.95	0.93	0.94	0.95
2008	0.67	0.61	0.64	0.65
2009	0.76	0.82	0.79	0.86
2010	0.84	0.72	0.77	0.82
2011	0.96	0.80	0.87	0.89
2012	0.93	0.79	0.86	0.89
2013	0.87	0.75	0.80	0.88
2014	0.94	0.74	0.83	0.91
2015	0.99	0.82	0.90	0.94
2016	0.87	0.89	0.88	0.95
2017	0.76	0.74	0.75	0.85
2018	0.92	0.87	0.89	0.92
2019	0.99	0.76	0.86	0.93

Explanations: PA = Producer's Accuracy, UA = User's Accuracy, IoU = Intersection over Union.
Source: own study.

SPATIOTEMPORAL DISTRIBUTION OF LAKE INUNDATION AREA IN 1989–2019

Figure 2 presents 29 maps of the annual lake inundation area during 1989–2019. The map was generated from the automation of the inundation extraction process by using water index in the GEE interface. The blue polygon in the figure indicates the presence of water and acts as the border of the lake inundation area; image composite was used as a background image. On top of that, the size of the inundation area was different in each observation year. The largest inundation area (3023.80 ha) was found in 1989, while the smallest inundation area was in 2016, at 971.90 ha. Based on the Mann–Kendall test, the inundation area of Lake Limboto showed a significantly decreasing trend at the significance level of 0.01 (p-value = 0.00008) over the last 30 years (Fig. 3). Overall, the area of the lake which has shrunk from 1989 to 2019 was 1933.74 ha.

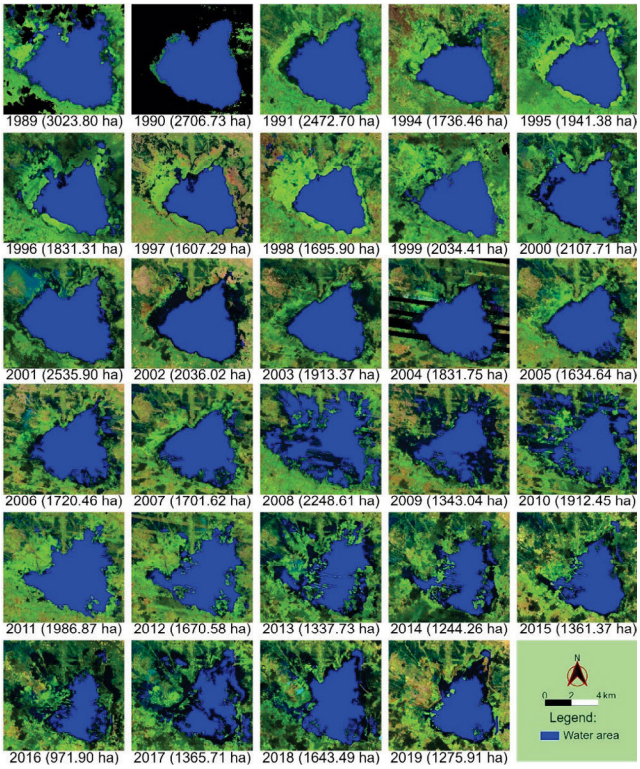

Fig. 2. Spatiotemporal variation of Lake Limboto inundation extent from 1989 to 2019; each image uses a band combination of near-infrared (NIR), red (R), and green (G); source: own study

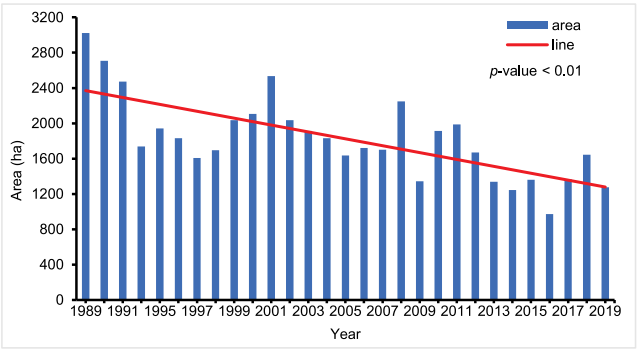

Fig. 3. The temporal variation of the inundated area from 1989 to 2019; source: own elaboration

DISCUSSION

Water index is an index that is often used to map the dynamics of changes in lake inundation, and previous studies have mainly used remote sensing images to calculate inundation area changes [Acharya *et al.* 2018; Eraku *et al.* 2019; Jiang *et al.* 2014]. In this study, to get a better understanding of the long-term changes in Lake Limboto, all the available Landsat images from 1989 to 2019 were used and analysed with the same index.

This study used a different approach to investigate the spatial-temporal variation of inundation areas in Lake Limboto

during 1989–2019. The use of the GEE as a cloud computing-based geospatial technology provides a flexible and efficient way to map the inundation area in Limboto Lake from 1989 to 2019. This work involves many images; however, these could be processed quickly without having to download the images. The GEE platform is capable of processing and analysing data in huge size and quantity [Gorelick *et al.* 2017]. Meanwhile, the approach in the previous study still required downloading of data for further local processing. Such a method would demand longer processing times and greater processing capacity if a series of satellite imagery were to be involved. Thus, this is considered inefficient [Nguyen *et al.* 2019]. Furthermore, the use of GEE technology in this study can save a lot of time when processing and analysing data.

As in previous studies on the long-term variation in the Lake Limboto inundation area [Hamzah *et al.* 2018; Kimijima *et al.* 2020], this study found a decrease in the annual area of the lake. The difference between this study and the previous study is that the spatial and temporal variation of shrinkage was specified each year in this study. Regarding the spatial variations, maps of annual inundation areas in Lake Limboto from 1989 to 2019 were made as an illustration. It is clearly apparent that the areas where the largest shrinkage occurred were in the western and north-western regions. This fact is probably related to the close geographical relationship with the three major rivers (Marisa, Alopuhu, and Meluopo) that flow into Lake Limboto. This is presumably due to these rivers' capability of loading sedimentary material into the lake. Besides, JICA [2002] reported that the Meluopo and Alopohu Rivers were the largest sediment contributors to the lake. The shrunk area has the potential to be converted into other land uses such as agricultural land and plantations, as reported by Umar *et al.* [2018]. Meanwhile, the temporal variation of inundation areas in Lake Limboto shows a significant decreasing trend during 1989–2019. Since this study used time-series data, it is possible to calculate the significance of trends that were not done in previous studies. The increasing shrinkage of the lake area will decrease the function of the lake as a water reservoir; thus increasing the risk for flooding around the lake area or even outside the lake. Therefore, the findings of the study are regarded as valid to provide information to the authorities to take anticipatory steps in Lake Limboto management in the future.

Several factors have been argued by previous studies to be the cause of shrinking inundation in Limboto Lake. The factors are rate of sedimentation, growth of aquatic vegetation, and land-use changes around the lake [Subehi *et al.* 2016; Umar *et al.* 2018]. The shrinkage phenomenon blames the massive rate of sedimentation as a result of a shift in land use at the Limboto watershed [JICA 2002]. Land-use change, especially the reduction of forest area, may contribute to sedimentation and erosion rates. Kimijima *et al.* [2020] reported that the high rate of sedimentation that enters Lake Limboto through rivers is mostly due to the erosion of the main rivers. Furthermore, the existence of aquatic vegetation, which has covered 43% of the lake surface as reported by KLHK [2015], could threaten the lake environment. The growth of aquatic vegetation increases due to eutrophication [Subehi *et al.* 2016]. According to Jaskuła and Sojka [2019], uncontrolled growth of aquatic vegetation can threaten the lake environment and gradually cause the lake area to decrease. In addition to that, the increased activities of agriculture, fisheries, and settlement development [Putra *et al.* 2013] also contributed to the sedimentation rate at the lake [Yunginger *et al.* 2018], and in turn, damaged the lake environment.

Further analysis on the climate variability during 1989–2019 would help to better understand the reasons for the shrinkage of the lake area. This climate variability can lead to a drought period [Chen, Yang 2013] and impacts the surface water level [Zou *et al.* 2017]. That being mentioned, the drought phenomenon, in its relation to the lake's spatial and temporal variation, is seen as an essential topic to explore further [Wu, Liu 2014]. On top of that, the drought period that occurred at the drainage basin of Lake Limboto during 1981–2016 [Koem, Rusiyah 2017; 2018] and its correlation with the dynamics of the lake's inundation during 1989–2019 is potential for further studies to investigate on.

There are several limitations to this study. Firstly, extraction of inundated areas did not consider the presence of aquatic vegetation as part of the lake area. Even so, the results in Figure 2 show that vegetation objects in the study area could be detected using the *NDVI* and *NDWI* indices. The light green on 1991, 1994, 1995, and 1998 images indicates the presence of vegetation. According to Trisakti [2013], some of the vegetation were part of the lake. However, in this study, the inundation area extraction was only carried out on objects identified as water. The authors were difficult to distinguish the boundary between terrestrial and aquatic vegetation, relying only on spectral information from the satellite data used. The spectral characteristics of aquatic vegetation are strongly influenced by atmospheric conditions and water effects [Zhou *et al.* 2018]. Besides, field measurement data to validate aquatic vegetation objects in the study area were not available.

Another limitation is the spatial resolution of the satellite data used in this study. The Landsat images employed have a spatial resolution of 30 m × 30 m, so the area of objects less than 30 m could not be detected. Additionally, The Landsat 7 ETM + images collected after 31 May 2003 have scan line errors. These images influenced the classification process, as shown in Figure 2 (images from 2004 to 2012). Further studies may as well involve data from remote sensing active technology and imagery from other satellites.

CONCLUSIONS

The study has shown that the water index method at the GEE platform is applicable to map out an inundation of a lake for a long period. The whole procedures (pre-processing, processing, analysis, and evaluation) were automatized by using the GEE interface; this is aimed to resolve the limitations found in conventional methods of satellite data processing. On top of that, the GEE data catalog also features satellite data from other sources; this feature allows a researcher to compare the mapping results and the dataset as previously mentioned. Such a method is highly useful in a condition in which other reference data or field data are not available.

Further, the lake inundation map obtained by the present work is applicable to support the prioritised sustainable management program of Lake Limboto. The dynamics of inundation in Lake Limboto are required to be simulated with the drought phenomenon in the lake's drainage basin as the aftermath of global climate fluctuation. Further studies might need to take into

account the water vegetation that covers the lake surface. Implementation of appropriate bands might be beneficial to detect the presence of any water vegetation on the lake. Further studies may as well involve image microwave sensors or high-resolution images.

REFERENCES

Acharya T., Subedi A., Lee D. 2018. Evaluation of water indices for surface water extraction in a Landsat 8 scene of Nepal. Sensors. Vol. 18, 2580. DOI 10.3390/s18082580.

Amani M., Ghorbanian A., Ahmadi S.A., Kakooei M., Moghimi A., Mirmazloumi S.M., ..., Brisco B. 2020. Google Earth Engine Cloud Computing Platform for remote sensing big data applications: A comprehensive review. IEEE Journal of Selected Topics in Applied Earth Observations and Remote Sensing. Vol. 13 p. 5326–5350. DOI 10.1109/JSTARS.2020.3021052.

Bolanos S., Stiff D., Brisco B., Pietroniro A. 2016. Operational surface water detection and monitoring using Radarsat 2. Remote Sensing. Vol. 8, 285. DOI 10.3390/rs8040285.

Buma W., Lee S.-I., Seo J. 2018. Recent surface water extent of Lake Chad from multispectral sensors and GRACE. Sensors. Vol. 18, 2082. DOI 10.3390/s18072082.

Chen Z., Yang G. 2013. Analysis of drought hazards in North China: Distribution and interpretation. Natural Hazards. Vol. 65 p. 279–294. DOI 10.1007/s11069-012-0358-3.

Clinton N. 2017. Otsu's method for image segmentation [online]. [Access 28.07.2020]. Available at: https://medium.com/google-earth/otsus-method-for-image-segmentation-f5c48f405e

Dinka M.O., Chaka D.D. 2019. Analysis of land use/land cover change in Adei watershed, Central Highlands of Ethiopia. Journal of Water and Land Development. No. 41 (IV–VI) p. 146–153. DOI 10.2478/jwld-2019-0038.

Du Y., Zhang Y., Ling F., Wang Q., Li W., Li X. 2016. Water bodies' mapping from Sentinel-2 imagery with modified Normalized Difference Water Index at 10-m spatial resolution produced by sharpening the SWIR band. Remote Sensing. Vol. 8. Iss. 4, 354 p. 1–19. DOI 10.3390/rs8040354.

Eraku S., Akase N., Koem S. 2019. Analyzing Limboto Lake inundation area using Landsat 8 OLI imagery and rainfall data. Journal of Physics: Conference Series. Vol. 1317, 012111. DOI 10.1088/1742-6596/1317/1/012111.

Google Earth Engine 2020. NDVI, mapping a function over a collection, quality mosaicking [online]. [Access 02.08.2020]. Available at: https://developers.google.com/earth-engine/tutorials/tutorial_api_06.

Gorelick N., Hancher M., Dixon M., Ilyushchenko S., Thau D., Moore R. 2017. Google Earth Engine: Planetary-scale geospatial analysis for everyone. Remote Sensing of Environment. Vol. 202 p. 18–27. DOI 10.1016/j.rse.2017.06.031.

Hamzah R., Matsushita B., Takehiko F. 2018. Long-term monitoring of lake surface area change in Indonesia from global surface water data [online]. In: 17th World Lake Conference. Ibaraki, Japan p. 600–602. [Access 02.08.2020]. Available at: https://www.pref.ibaraki.jp/soshiki/seikatsukankyo/kasumigauraesc/04_kenkyu/kaigi/docments/kosyou/17/ronbun/WLC17procidings_O6_14.pdf

Hardy A., Ettritch G., Cross D.E., Bunting P., Liywalii F., Sakala J., Silumesii A., Singini D., Smith M., Willis T., Thomas C.J. 2019. Automatic detection of open and vegetated water bodies using Sentinel 1 to map African malaria vector mosquito breeding habitats. Remote Sensing. Vol. 11, 593. DOI 10.3390/rs11050593.

Huang C., Chen Y., Zhang S., Wu J. 2018. Detecting, extracting, and monitoring surface water from space using optical sensors: A review. Reviews of Geophysics. Vol. 56 p. 333–360. DOI 10.1029/2018RG000598.

Jaskuła J., Sojka M.. 2019. Assessing spectral indices for detecting vegetative overgrowth of reservoirs. Polish Journal of Environmental Studies. Vol. 28. No. 6 p. 4199–4211. DOI 10.15244/pjoes/98994.

Jiang H., Feng M., Zhu Y., Lu N., Huang J., Xiao T. 2014. An automated method for extracting rivers and lakes from Landsat imagery. Remote Sensing. Vol. 6. Iss. 6 p. 5067–5089. DOI 10.3390/rs6065067.

JICA 2002. The study on flood control and water management Limboto-Bolango-Bone Basin in The Republic of Indonesia [online]. Final report. Vol. 1. Summary. Japan International Cooperation Agency. [Access 02.08.2020]. Available at: https://openjicareport.jica.go.jp/pdf/11709730_01.pdf

Kendall M.G. 1975. Rank correlation methods. 4th ed. London. Griffin. ISBN 0852641990 pp. 202.

Kimijima S., Sakakibara M., Amin A.K.M.A., Nagai M., Indriati A.Y. 2020. Mechanism of the rapid shrinkage of Limboto Lake in Gorontalo, Indonesia. Sustainability. Vol. 12. Iss. 22, 9598. DOI 10.3390/su12229598.

KLHK 2015. Gerakan penyelamatan danau Limboto (Germadan Limboto) [Lake rescue movement of Limboto Lake]. Gorontalo. Kementerian Lingkungan Hidup dan Kehutanan pp. 91.

Koem S., Rusiyah 2017. Monitoring of drought events in Gorontalo Regency. IOP Conference Series: Earth and Environmental Science. Vol. 98, 012053. DOI 10.1088/1755-1315/98/1/012053.

Koem S., Rusiyah 2018. Karakteristik spasiotemporal kekeringan meteorologi di Kabupaten Gorontalo tahun 1981–2016 [Spatio-temporal characteristics of meteorological drought in Gorontalo Regency in 1981–2016]. Jurnal Pengelolaan Sumberdaya Alam dan Lingkungan. Vol. 8 p. 355–364. DOI 10.29244/jpsl.8.3.355-364.

Kumar L., Mutanga O. 2018. Google Earth Engine applications since inception: Usage, trends, and potential. Remote Sensing. Vol. 10, p. 1509. DOI 10.3390/rs10101509.

Mann H.B. 1945. Nonparametric tests against trend. Econometrica. Vol. 13. No. 3 p. 245–259. DOI 10.2307/1907187.

Maxwell A.E., Warner T.A. 2020. Thematic classification accuracy assessment with inherently uncertain boundaries: An argument for Center-Weighted Accuracy Assessment Metrics. Remote Sensing. Vol. 12, 1905. DOI 10.3390/rs12121905.

McFeeters S.K. 1996. The use of the Normalized Difference Water Index (NDWI) in the delineation of open water features. International Journal of Remote Sensing. Vol. 17 p. 1425–1432. DOI 10.1080/01431169608948714.

Nguyen U.N.T., Pham L.T.H., Dang T.D. 2019. An automatic water detection approach using Landsat 8 OLI and Google Earth Engine cloud computing to map lakes and reservoirs in New Zealand. Environmental Monitoring and Assessment. Vol. 191, 235. DOI 10.1007/s10661-019-7355-x.

Okoro S.U., Schickhoff U., Böhner J., Schneider U.A. 2016. A novel approach in monitoring land-cover change in the tropics: Oil palm cultivation in the Niger Delta, Nigeria. DIE ERDE – Journal of the Geographical Society of Berlin. Vol. 147(1) p. 40–52. DOI 10.12854/erde-147-3.

Otsu N. 1979. A threshold selection method from gray-level histograms. IEEE Transactions on Systems, Man, and Cybernetics. Vol. 9 p. 62–66. DOI 10.1109/TSMC.1979.4310076.

Pekel J.-F., Cottam A., Gorelick N., Belward A.S. 2016. High-resolution mapping of global surface water and its long-term changes. Nature. Vol. 540 p. 418–422. DOI 10.1038/nature20584.

Putra S.S., Hassan C., Djudi, Suryatmojo H. 2013. Reservoir saboworks solutions in Limboto Lake Sedimentations, Northern Sulawesi, Indonesia. Procedia Environmental Sciences. Vol. 17 p. 230–239. DOI 10.1016/j.proenv.2013.02.033.

Rezzag Bara C., Djidel M., Medjani F., Labar S. 2019. Spatiotemporal evolution of land surface temperature of Lake Oubeira catchment, northeastern Algeria. Journal of Water and Land Development. No. 43 (X–XII) p. 151–157. DOI 10.2478/jwld-2019-0073.

Rouse W., Haas H., Deering W. 1973. Monitoring vegetation systems in the great plains with ERTS. In: 3rd Earth Resources Technology Satellite-1 Symposium. NASA. Vol. 1 p. 309–317.

Sen P.K. 1968. Estimates of the regression coefficient based on Kendall's Tau. Journal of the American Statistical Association. Vol. 63(324) p. 1379. DOI 10.2307/2285891.

Stuhler S.C., Leiterer R., Joerg P.C., Wulf H., Schaepman M.E. 2016. Generating a cloud-free, homogeneous Landsat-8 mosaic of Switzerland using Google Earth Engine. DOI 10.13140/RG.2.1.2432.0880.

Subehi L., Wibowo H., Jung K. 2016. Characteristics of rainfall-discharge and water quality at Limboto Lake, Gorontalo, Indonesia. Journal of Engineering and Technological Sciences. Vol. 48 p. 288–300. DOI 10.5614/j.eng.technol.sci.2016.48.3.4.

Tamiminia H., Salehi B., Mahdianpari M., Quackenbush L., Adeli S., Brisco B. 2020. Google Earth Engine for geo-big data applications: A meta-analysis and systematic review. ISPRS Journal of Photogrammetry and Remote Sensing. Vol. 164 p. 152–170. DOI 10.1016/j.isprsjprs.2020.04.001.

Trisakti B. 2013. Kajian penentuan luas permukaan air danau dan sebaran vegetasi air dengan metoda penginderaan jauh [Study of the lake water surface area and aquatic vegetation distribution determination based on remote sensing method]. LIMNOTEK. Vol. 20. No. 1 p. 10–20.

Umar I., Marsyoyo A., Setiawan B. 2018. Analisis Perubahan Penggunaan Lahan Sekitar Danau Limboto Di Kabupaten Gorontalo [Analysis of changes in land use around Limboto Lake in Gorontalo District]. Jurnal Tata Kota dan Daerah. Vol. 10. No. 2 p. 77–90. DOI 10.21776/ub.takoda.2018.010.02.3.

Wang C., Jia, M., Chen N., Wang W. 2018. Long-term surface water dynamics analysis based on Landsat imagery and the Google Earth Engine platform: A case study in the Middle Yangtze River Basin. Remote Sensing. Vol. 10, 1635. DOI 10.3390/rs10101635.

Wang Y., Li Z., Zeng C., Xia G.-S., Shen H. 2020. An urban water extraction method combining deep learning and Google Earth Engine. IEEE Journal of Selected Topics in Applied Earth Observations and Remote Sensing. Vol. 13 p. 769–782. DOI 10.1109/JSTARS.2020.2971783.

Wang Y., Ma J., Xiao X., Wang X., Dai S., Zhao B. 2019. Long-term dynamic of Poyang Lake surface water: A mapping work based on the Google Earth Engine cloud platform. Remote Sensing. Vol. 11, 313. DOI 10.3390/rs11030313.

Wu G., Liu Y. 2014. Satellite-based detection of water surface variation in China's largest freshwater lake in response to hydro-climatic drought. International Journal of Remote Sensing. Vol. 35 p. 4544–4558. DOI 10.1080/01431161.2014.916444.

Yunginger R., Bijaksana S., Dahrin D., Zulaikah S., Hafidz A., Kirana K., Sudarningsih S., Mariyanto M., Fajar S. 2018. Lithogenic and anthropogenic components in surface sediments from Lake Limboto as shown by magnetic mineral characteristics, trace metals, and REE geochemistry. Geosciences. Vol. 8 p. 116. DOI 10.3390/geosciences8040116.

Zhou G., Ma Z., Sathyendranath S., Platt T., Jiang C., Sun K. 2018. Canopy reflectance modeling of aquatic vegetation for algorithm development: Global sensitivity analysis. Remote Sensing. Vol. 10. Iss. 6, 837 p. 1–22. DOI 10.3390/rs10060837.

Zou Z., Dong J., Menarguez M.A., Xiao X., Qin Y., Doughty R.B., Hooker K.V., Hambright K.D. 2017. Continued decrease of open surface water body area in Oklahoma during 1984–2015. Science of The Total Environment. Vol. 595 p. 451–460. DOI 10.1016/j.scitotenv.2017.03.259.